Dosimetric study of bevel factors in IOERT with mobile linacs: towards a unified code of practice

Rafael Ayala[a,b], Rocío García[a], Gema Ruiz[a], María Jesús García[a], Álvaro Soza[a], Susana Gómez[a], José Manuel Udías[b,c], Paula Ibáñez[b,c]

[a] *Servicio de Dosimetría y Radioprotección, Hospital General Universitario Gregorio Marañón, Dr. Esquerdo 46, 28007, Madrid, Spain*

[b] *Nuclear Physics Group and IPARCOS, Department of Structure of Matter, Thermal Physics and Electronics, CEI Moncloa, Universidad Complutense de Madrid, Madrid, Spain*

[c] *Instituto de Investigación Sanitaria del Hospital Clínico San Carlos, Madrid, Spain*

Abstract

Background: Dosimetry in intraoperative electron radiotherapy (IOERT) poses distinct challenges, especially with inclined applicators deviating from international protocols. Ion recombination in ionization chambers, electron beam degradation due to scattering in cylindrical applicators, coupled with a lack of a well-defined beam quality surrogate, complicate output factor determination with ionization chambers. Synthetic diamond-based detectors, offer potential solutions; however, their suitability requires further exploration.
Purpose: This study addresses output factor determination for beveled applicators. Objectives include assessing the suitability of PTW microDiamond detectors and determining correction factors for ionization chamber measurements based on energy variations at the depth of maximum dose (z_{max}) for beveled applicators. Experimental data are compared against results obtained from Monte Carlo simulations.
Methods: We conducted measurements using both PTW microDiamond and IBA CC01 detectors. In addition to benchmarking bevel factors with penEasy, we employed Monte Carlo simulations to determine angular response correction factors for microDiamond detectors and to evaluate energy variations at z_{max} for beveled applicators.
Results: The findings indicate that angular response correction factors are

Email address: rafael.ayala@salud.madrid.org (Rafael Ayala)

unnecessary for microDiamond detectors with beveled applicators. However, variations in mean energy at z_{max} potentially impact absorbed dose calculations with ionization chambers, particularly with the most inclined applicators.
Conclusions: Based on our results, the study recommends using microDiamond detectors over cylindrical ionization chambers for output factor determination in IOERT with inclined applicators. Addressing energy variations at z_{max} is crucial to improve accuracy in ionization chamber measurements. These findings have implications for dosimetry protocols in IOERT, contributing to enhanced delivery in clinical practice.

---

1. Introduction

Intraoperative radiotherapy (IORT) has emerged as a valuable adjuvant to surgical oncology, offering precise and localized radiation delivery directly to the tumor or tumor bed during surgery. Its unique advantage lies in the ability to visually assess the target volume and selectively spare adjacent healthy tissues, thereby maximizing the absorbed dose to the target volume while minimizing the absorbed dose to normal tissue.

Among the different techniques available in IORT, intraoperative electron radiotherapy (IOERT) consists of delivering high-energy electrons using a linear accelerator. The evolution of IOERT has progressed from transporting patients from the surgical room to a conventional linear accelerator to the utilization of dedicated mobile accelerators capable of delivering prescribed doses directly in the surgical room.

However, the benefits of IOERT come with a major caveat: dosimetry in intraoperative electron radiotherapy (IOERT), especially with mobile accelerators, deviates in several aspects from the recommendations of international protocols [1, 2]. Mobile IOERT linacs are characterized by a particularly high dose per pulse which is desirable to provide faster treatments, but also causes additional dosimetric problems when determining absorbed dose with ionization chambers. The effect of ion recombination has been extensively studied in the literature for plane-parallel chambers [3, 4, 5] and, to a certain extent, for cylindrical chambers as well [6].

In addition to that, electron beams are known to be affected by scattering in the cylindrical applicators and, as such, they have been referred to as degraded beams [7]. The effect of scattering on stopping-power ratios, which are a fundamental part of absorbed dose determination with ionization chambers, has been studied for standard [8] and mobile linacs [9, 10], the latter

having slightly different spectral shapes, especially at shallow depths, due to the absence of bending magnets [11]. In both cases, the use of tabulated stopping-power ratios [12] results in a relatively small additional contribution to the total uncertainty budget.

While efforts have been made to establish guidelines for the IORT technique and dosimetry [13, 14], certain unresolved issues persist, particularly those related to inclined applicators. Beveled applicators are essential for enhancing target conformity and adapting to patient anatomy. However, they inevitably produce oblique incidences (see Fig. 1), leading to several additional challenges in accurately determining absorbed dose with ionization chambers.

In this regard, cylindrical ionization chambers are particularly advantageous due to their inherent insensitivity to beam direction. However, it is important to consider the size of the chambers. Large cylindrical chambers can experience significant saturation and volume effects in the presence of high dose gradients and doses per pulse typical of mobile IOERT linacs. In contrast, small cylindrical chambers with a small radius provide high spatial resolution and reduced ion recombination effects [6].

Nevertheless, selecting the most suitable ionization chamber does not completely solve the problem of determining the absorbed dose with beveled applicators. There is a more fundamental issue that arises from the lack of a well defined beam quality surrogate. The half value depth (R_{50}) of percentage depth dose curves (PDDs) in oblique beams can be determined along the clinical or the geometrical axis, corresponding to the direction perpendicular to the water surface and the direction of the incident beam, respectively. While the clinical axis is perceived as more relevant to IOERT as it determines the depth of the volume of interest to be irradiated during

Fig. 1: Typical setup for determining output factors with a beveled applicator.

treatment [13], neither approach provides a reasonable characterization of the mean energy of the beam at the point of measurement. Therefore, new strategies need to be followed to address this limitation. One possibility would be to assume that the energy spectrum at the depth of maximum dose (z_{max}) of the beveled applicator is the same as that of the flat applicator at the same depth. However, this remains to be proven and it is one of the objectives of this paper.

Most of the aforementioned challenges can be addressed by using solid-state detectors that are independent of dose rate, with synthetic diamond-based detectors being suitable options. Synthetic diamond detectors offer several advantages, including nearly constant and close-to-unity water-to-carbon stopping-power ratios across the relevant energy ranges [15]. Moreover, these detectors exhibit high depth resolution [16]. Previous studies

conducted by Di Venanzio et al. and Güngör et al. [17, 18], have already investigated the applicability of PTW microDiamond detectors for relative measurements in IOERT. However, it is important to note that microDiamond detectors exhibit an inhomogeneous angular response for photons [19] and, for IOERT measurements with oblique incidences, it has been proposed that correction factors should be applied [20].

On the modeling and simulation sides, Monte Carlo calculations already play an important role in IOERT due to their significance in accurately predicting dose distributions either where detailed geometries are known [11, 9] or they are derived from reconstructed Phase-Space Files [21]. In this paper, we will utilize Monte Carlo simulations as a benchmark to compare bevel factor measurements with a small ionization chamber (IBA CC01) and a synthetic diamond detector (PTW microDiamond). Additionally, these simulations will be employed to investigate potential changes in the electron energy spectrum, providing valuable insights into the measurement of electron beams with ionization chambers. Furthermore, we propose correction factors for ionization chambers to account for differences in mean energy at the point of measurement for beveled applicators and we analyze the effect of the previously derived angular corrections for the PTW microDiamond [20]. These angular corrections are derived from an experimental setup involving a flat applicator moved around a water sphere while keeping the detector in place. However, it's worth noting that this setup might not precisely correspond to an inclined applicator impinging on a flat water surface. To address this potential discrepancy, we conducted Monte Carlo simulations to compare both scenarios. Our goal is to enhance the understanding of IOERT beams through Monte Carlo simulations, aiming for more precise dosimetry. This effort contributes to the advancement of treatment planning and delivery in

clinical practice.

The existing literature on inclined applicators is limited [6, 22], and we believe that, despite its direct impact on IOERT treatments, the specific challenges associated with characterizing inclined applicators have not been sufficiently addressed. In our institution almost 80% of the patients have been treated with beveled applicators and more than 43% with a 45° applicator ending (Fig. 2). These significant numbers emphasize the widespread clinical relevance of understanding and accurately characterizing the dosimetric properties of inclined applicators. Addressing this gap in the literature is crucial to ensure optimal treatment planning and delivery in IOERT, enhancing the overall quality and effectiveness of patient care.

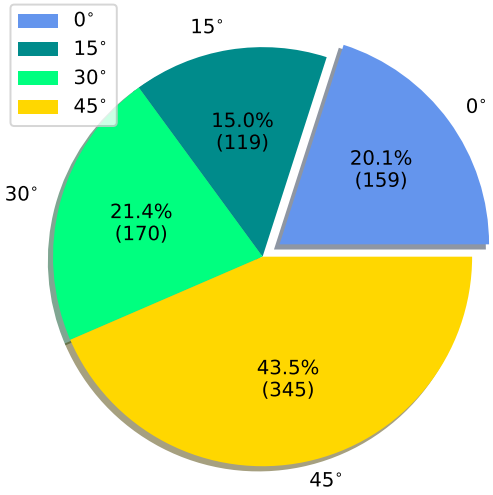

Fig. 2: Distribution of bevel angles in 793 IEORT treatments with a Liac 12 MeV (SIT). Only 20.1% of the total treatments were delivered with a flat applicator. 43.5% were delivered with the most inclined applicator (45°).

2. Material and Methods

2.1. Beam characteristics and detectors

All measurements were performed on a mobile IOERT linac Liac 12 MeV model (SIT). The nominal energies are 6, 8, 10 and 12 MeV, corresponding to pulse rate frequencies (PRFs) of 20, 15, 10 and 10 Hz, respectively.

The linac uses a hard docking system with applicators consisting of polymethyl methacrylate (PMMA) cylinders with inner diameters 3, 4, 5, 6, 7, 8, 10 and 12 cm. Each applicator, in turn, can have different endings with four different bevel angles 0, 15, 30 and 45 degrees. Throughout this paper, an applicator of diameter d (in cm) and bevel angle α (in degrees) will be referred to as $C_d B_\alpha$.

Additional beam characteristics can be found in Table 1.

Table 1: Beam characteristics of the reference applicator $C_{10}B_0$.

	Beam characteristics $C_{10}B_0$			
Energy (MeV)	6	8	10	12
PRF (Hz)	20	15	10	10
Dose per pulse (cGy/p)	0.6	1.3	2.5	3.5
z_{max} (cm)	0.8	1.1	1.3	1.4
R_{50} (cm)	2.3	3.0	3.9	4.5

The accelerator output is determined, to the extent possible, following the IAEA TRS-398 dosimetry protocol [1], using an IBA PPC05 parallel-plate ionization chamber. Although the 2024 version of TRS-398 [1] provides $k_{Q,Q_{int}}$ energy correction factors for the PPC05 ionization chamber based on

Muir et al. [23], the $k_{Q,Q_{int}}$ values utilized in this study were derived from data published by Sempau et al. [24].

Recombination factors (k_{sat}) were calculated following Laitano method [3] using the third of the Boag's models [25]. The linac is calibrated to deliver 1 cGy per monitor unit (MU) at z_{max} of the $C_{10}B_0$ applicator for all four energies.

The smallest applicator, with a diameter of 3 cm, delivers the highest dose per pulse (6.2 cGy/p) when paired with a 45° bevel ending and a 12 MeV beam energy.

All measurements and calculations were performed in water at different depths along the clinical axis.

While the PPC05 ionization chamber is suitable for linac calibration, it may present challenges with oblique incidences and small applicators, necessitating the use of alternative detectors. In this study, the determination of output factors will involve the use of the IBA CC01 and PTW microDiamond detectors.

2.1.1. IBA CC01

The IBA CC01 detector is a cylindrical ionization chamber with a cavity volume of 0.01 cm^3 and a cavity radius of 1 mm. The wall material is C552 and the central electrode is made of steel. The effect of high-Z electrodes in ionization chambers has been studied by Muir and Rogers [26] finding large variations in central electrode correction factors (P_{cel}) for photons, although for electrons P_{cel} variations were found to be small (<0.2% for R_{50} variations of 4 cm). The effect of P_{cel} is therefore considered to be negligible in the present work.

k_{sat} values for this chamber were calculated using Karaj method [6] and polarization effects (k_{pol}) were assessed by the recommended two-voltage TRS-398

procedure [1].

2.1.2. Synthetic diamond detector

The PTW microDiamond 60019 is a synthetic diamond detector manufactured by chemical vapor deposition (CVD). It is constructed with a 7 mm diameter outer cap and a sensitive circular area measuring 2.2 mm in diameter and 1 μm in thickness [16]. The active volume is at 1 mm water-equivalent depth from the outer surface. To avoid the need to apply an external polarization voltage, diamond detectors are designed as Schottky diodes, one of the electrodes is attached to an aluminium plate that creates a potential between the two materials. A previous study by Di Venanzio et al. [17] showed the suitability of this detector for IOERT beams with doses per pulse up to 10 cGy/p.

2.2. Monte Carlo simulation

Monte Carlo simulation of the Liac 12 MeV model was performed following the methodology of Iaccarino et al. [11] Instead of EGSnrc/BEAMnrc [27], the code penEasy 2020 [28], based on PENELOPE 2018 [29] has been used. The linac geometry was defined with the aid of the PENGEOM subroutines [30], specifically through the Java GUI PenGeomJar. Phase-Space Files (PSFs) were recorded just below the bevel junction of the C_dB_0 applicator (Fig. 3) using the tally Phase-Space File. These calculated PSFs were then used for simulating the four beveled applicators with the same diameter and beam energy. Spatial dose distributions were computed for each combination of energy, applicator diameter, and bevel angle. The results of the simulations were recorded in a cylindrical virtual water phantom of 50 cm diameter positioned directly beneath the applicator (Fig. 3), utilizing the Spatial Dose Distribution tally and requiring a statistical uncertainty of 0.5% (k=2).

The transport parameters for the various materials utilized in the simulations are detailed in Table 2. All transport parameters were set to their default values in penEasy, with the exception of DSMAX for materials comprising exit windows, scattering foil, applicators and monitor chambers. These values were specifically chosen to ensure adequate interaction of all particles within these components of the linac. As per PENELOPE documentation, a DSMAX of one-tenth of the thickness of a thin body is required to ensure reliability of the simulation algorithm [29]. However, for thicker materials, such as those used in the bulk of the linac or water, DSMAX was set to a very high value (10^{30}) to effectively disable step-length control, as the number of interactions in these thicker bodies is sufficient without additional step-length constraints. This approach ensures computational efficiency while maintaining accuracy where it is most critical.

Table 2: PENELOPE transport parameters for the materials used in penEasy simulations. Refer to Iaccarino et al. [11] for a detailed description of the geometry and materials of the Liac 12MeV. DSMAX values of 10^{30} indicate that step-length control is effectively disabled for these materials, as sufficient interactions occur without this constraint, particularly in thicker materials.

Material	EABS (e^- and e^+) (eV)	EABS (ph) (eV)	C_1	C_2	W_{cc} (eV)	W_{cr} (eV)	DSMAX (cm)
Air	10^5	10^4	0.1	0.1	$1.4{\cdot}10^5$	$1.4{\cdot}10^4$	10^{30}
Aluminium	10^5	10^4	0.1	0.1	$1.4{\cdot}10^5$	$1.4{\cdot}10^4$	10^{-4}
PEEK	10^5	10^4	0.1	0.1	$1.4{\cdot}10^5$	$1.4{\cdot}10^4$	10^{30}
PMMA	10^5	10^4	0.1	0.1	$1.4{\cdot}10^5$	$1.4{\cdot}10^4$	10^{-2}
Titanium	10^5	10^4	0.1	0.1	$1.4{\cdot}10^5$	$1.4{\cdot}10^4$	10^{-4}
Water	10^5	10^4	0.1	0.1	$1.4{\cdot}10^5$	$1.4{\cdot}10^4$	10^{30}

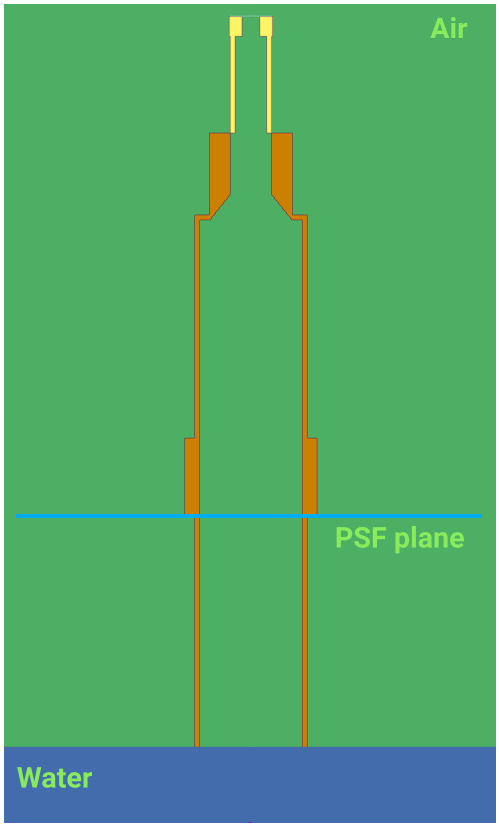

Fig. 3: PenGeomJar 2D visualization of the 10 cm flat applicator, PSF files were recorded in a plane just below the bevel junction. Each material is distinguished by a distinct color, with PMMA displayed in orange, PEEK in yellow, air represented in green, and water depicted in blue. The aluminum scattering foil is positioned just above the PEEK components.

2.2.1. Energy spectra at different depths

The energy spectra were calculated using a modified penEasy program where the tally Particle Current Spectrum was replicated nine times. This allowed the calculation of mean energy-vs-depth curves in a single simulation. The electron energies were recorded in 50 bins ranging from 0 to nominal energy plus 2 MeV in a cylindrical water volume with a radius of 1.5 mm and

a height of 0.1 mm. This extended energy range accounts for peaks in initial electron energy spectrum that are higher than the nominal energy [9, 11]. The requested statistical uncertainty was 1% (k=2) per each bin, resulting in less than 0.4% (k=2) for the average spectrum energy.

2.2.2. Absorbed dose for output factor determination

Absorbed doses were recorded using the tally Cylindrical Dose Distribution in cylindrical volumes of the same size as above. The required statistical uncertainty in the simulation was set at 0.5% (k=2).

2.2.3. Absorbed dose distributions in a water sphere

In order to better understand and compare previously published correction factors [20], the experimental setup from the study of Mastella et al. was replicated in Monte Carlo simulations. Absorbed dose distributions in a water sphere of 4 cm diameter with beam incidences at 0 and 45 degrees were compared with dose distributions of a flat and a 45° beveled applicator (Fig. 4). Similar to the previous section, the simulation was stopped when the statistical uncertainty of the simulation reached 0.5% (k=2).

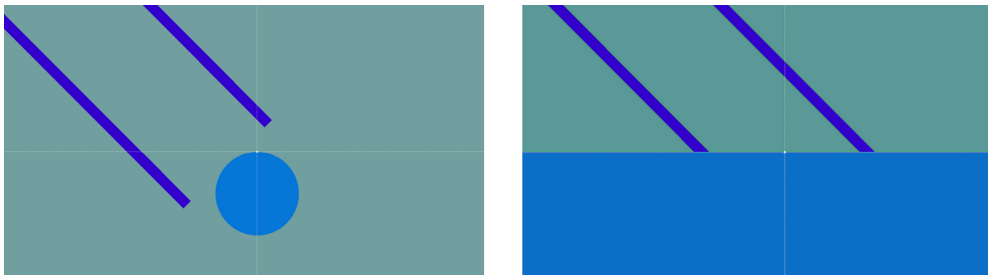

Fig. 4: PenGeomJar 2D visualizations of the C_5B_0 applicator with a 45° rotation around a 4 cm diameter water sphere (left) and the C_5B_{45} applicator with its bevel parallel to a flat water surface (right).

2.3. Ouput factors determination

For convenience, the output factors have been divided into two contributions, cylinder factor and bevel factor. Cylinder factors (CF_d) are defined as the ratio of the absorbed dose at z_{max} of a flat-ended applicator of diameter d and the reference applicator $C_{10}B_0$ for the same number of delivered monitor units.

$$CF_d = \frac{D_{C_dB_0}}{D_{C_{10}B_0}} \tag{1}$$

Bevel factors ($BF_{d,\alpha}$), in turn, are defined as the ratio of the absorbed dose at z_{max} of the beveled and the flat-ended applicators of the same diameter for the same number of delivered monitor units.

$$BF_{d,\alpha} = \frac{D_{C_dB_\alpha}}{D_{C_dB_0}} \tag{2}$$

Therefore, the total output factor is calculated according to Equation (3).

$$OF_{d,\alpha} = CF_d * BF_{d,\alpha} \tag{3}$$

Following the assumption that electron perturbation factors remain constant for either inclined and flat applicators, Equation (4) was employed for the determination of bevel factors with the microDiamond detector.

$$BF^{\mu D}_{d,\alpha} = \frac{M_{C_dB_\alpha}}{M_{C_dB_0}} \tag{4}$$

where $M_{C_dB_\alpha}$ is the reading of the electrometer when the detector is located at z_{max} of the clinical axis of the C_dB_α applicator.

Alternatively, if measured with CC01, bevel factors were calculated using Equation (5), which solely considers the change in electron energy spectrum due to the different depths of z_{max} in both flat and inclined applicators.

$$BF^{CC01}_{d,\alpha} = \frac{(M * k_{TP} * k_h * k_{elec} * k_{pol} * k_{sat} * k_{Q,Q_{cross}})_{C_dB_\alpha} * \frac{S_{w,air}(z_{max}C_dB_\alpha)}{S_{w,air}(z_{ref}C_dB_0)}}{(M * k_{TP} * k_h * k_{elec} * k_{pol} * k_{sat} * k_{Q,Q_{cross}})_{C_dB_0} * \frac{S_{w,air}(z_{max}C_dB_0)}{S_{w,air}(z_{ref}C_dB_0)}} \tag{5}$$

k values in Equation (5) correspond to correction factors for temperature and pressure (k_{TP}), humidity (k_h), electrometer (k_{elec}), polarity (k_{pol}) and saturation (k_{sat}). $S_{w,air}$ represent Spencer–Attix water-to-air stopping-power ratios calculated from R_{50} of the referred applicator and at the specified depth. Both $\frac{S_{w,air}(z_{max}C_dB_\alpha)}{S_{w,air}(z_{ref}C_dB_0)}$ and $\frac{S_{w,air}(z_{max}C_dB_0)}{S_{w,air}(z_{ref}C_dB_0)}$ terms appear in Equation (5) to take into account that, following TRS-398 recommendations [1], $k_{Q,Q_{cross}}$ values should be tabulated at z_{ref}, but measurements are performed at z_{max}. k_h and k_{elec} and $k_{Q,Q_{cross}}$ have been assumed to be constant in both measurements, therefore,

Equation (5) can be simplified as follows:

$$BF_{d,\alpha}^{CC01} = \frac{(M * k_{TP} * k_{pol} * k_{sat})_{C_dB_\alpha} * S_{w,air}(z_{max}C_dB_\alpha)}{(M * k_{TP} * k_{pol} * k_{sat})_{C_dB_0} * S_{w,air}(z_{max}C_dB_0)} \tag{6}$$

For Monte Carlo simulations, Equation (2) was directly applied.

2.3.1. Mean energy correction for ionization chambers

To address the potential variations in energy spectra at z_{max} between inclined and flat applicators, we suggest introducing a correction factor for ionization chamber measurements. This correction factor is derived from stopping-power ratios.

The mean energy of beams using applicators $C_{10}B_0$, C_5B_0 and C_3B_0 was calculated as a function of depth with Monte Carlo simulations.

After that, the depth $z_{0,\alpha}$ (Fig. 5) where $E_{z_{0,\alpha}}(C_dB_0) = E_{z_{max}}(C_dB_\alpha)$ was determined by linear interpolation, and using data from Burns et al. [31], new corrected $S_{w,air}(z_{0,\alpha})$ were applied in Equation (6) for each applicator diameter.

$$S_{w,air}(z_{0,\alpha}) = \frac{a + bx + cx^2 + dy}{1 + ex + fx^2 + gx^3 + hy} \tag{7}$$

where $x = \ln(R_{50})$ and $y = z_{0,\alpha}/R_{50}$, and the values for the constants from Burns et al. [31] are:

$$a = 1.075 \quad b = -0.5087 \quad c = 0.0887 \quad d = -0.084$$

$$e = -0.4281 \quad f = 0.0646 \quad g = 0.00309 \quad h = -0.125$$

R_{50} values correspond to half value depths of the flat applicator.

Equation (6) then becomes:

$$BF_{d,\alpha}^{CC01_{corr}} = \frac{(M * k_{TP} * k_{pol} * k_{sat})_{C_dB_\alpha} * S_{w,air}(z_{0,\alpha})}{(M * k_{TP} * k_{pol} * k_{sat})_{C_dB_0} * S_{w,air}(z_{max}C_dB_0)} \tag{8}$$

Which can be expressed as:

$$BF_{d,\alpha}^{CC01_{corr}} = BF_{d,\alpha}^{CC01} * \frac{S_{w,air}(z_{0,\alpha})}{S_{w,air}(z_{max}C_dB_\alpha)} \tag{9}$$

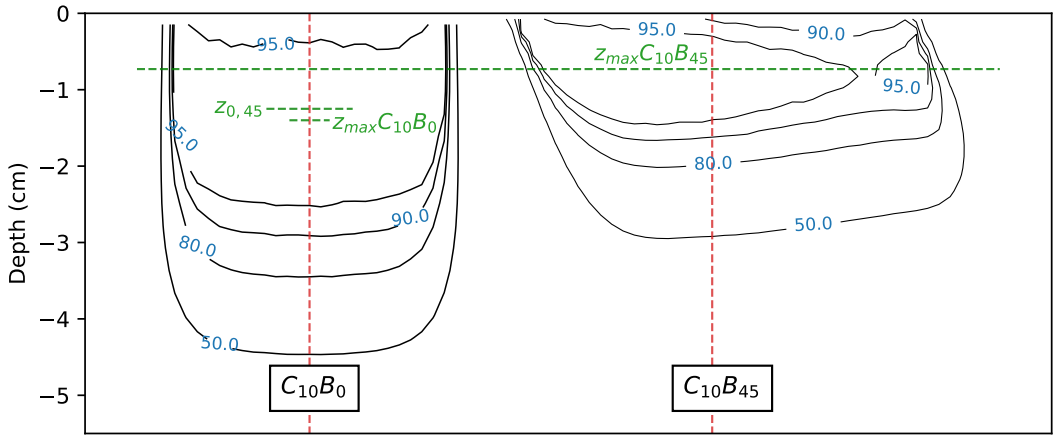

Fig. 5: Schematic representation of $z_{0,45}$ and z_{max} in 12 MeV isodose distributions in water for $C_{10}B_0$ and $C_{10}B_{45}$ applicators. Isodose levels are normalized to z_{max} along the clinical axis (in red) and expressed as percentages.

3. Results

3.1. Monte Carlo simulations

The agreement of the PDD curves and beam profiles between Monte Carlo simulations and microDiamond measurements can be observed in Fig. 6.

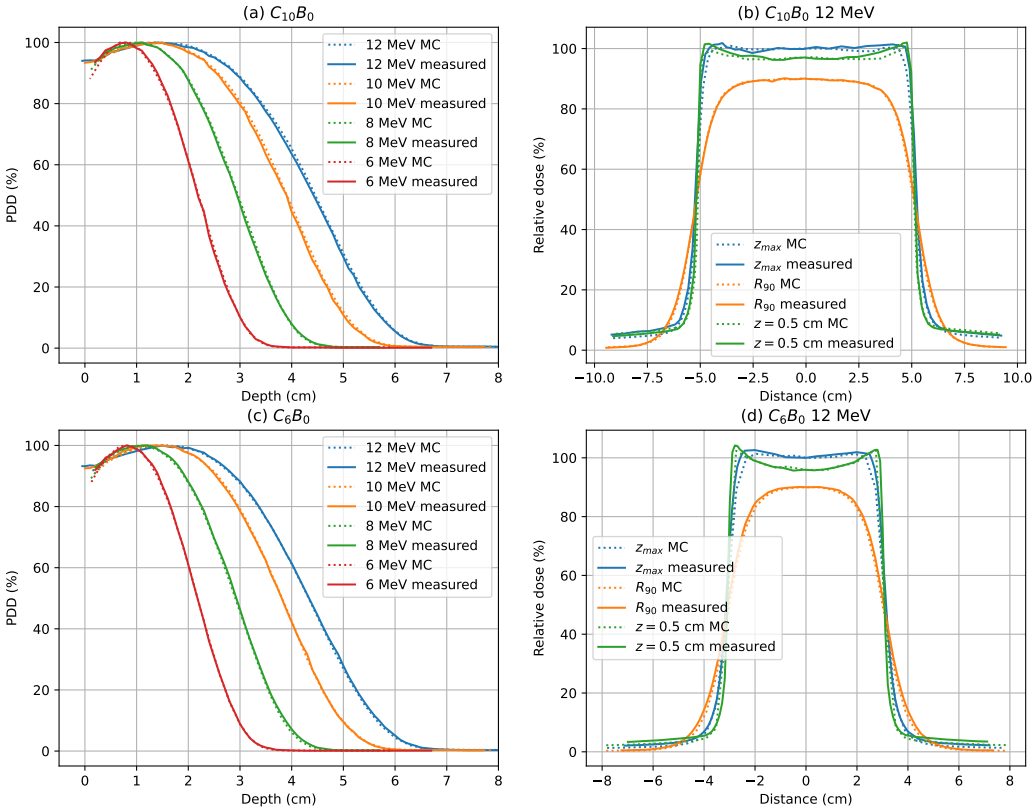

Fig. 6: PDD curves measured for the four different energy beams using the $C_{10}B_0$ applicator (a) and the C_6B_0 applicator (c), along with a comparison to Monte Carlo (MC) results. The measured profiles of the 12 MeV beam at depths of 0.5 cm, z_{max}, and R_{90} are shown for the $C_{10}B_0$ (b) and C_6B_0 (d) applicators, highlighting their agreement with the Monte Carlo simulations.

Fig. 7 illustrates the impact of oblique incidence from inclined applicators on absorbed dose distributions. As the bevel angle increases, the absorbed dose distributions of inclined applicators exhibit a reduction in electron range and a noticeable heel effect. It is noteworthy that even with high bevel angles,

the isodose curves remain almost parallel to the water surface.

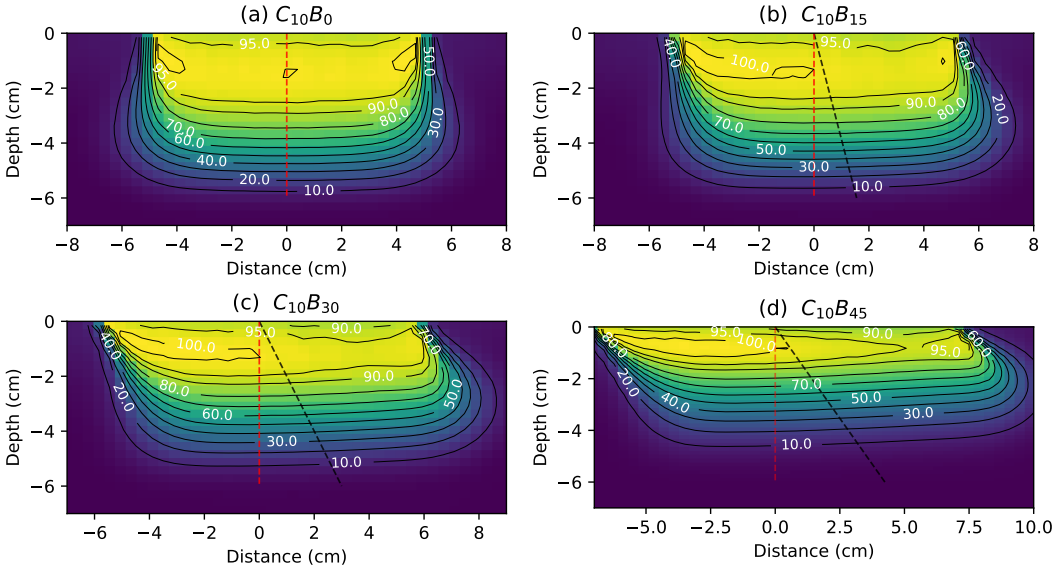

Fig. 7: Effect of increasing the bevel angle on absorbed dose distributions in water with a 12 MeV electron beam. The figure shows penEasy calculations for $C_{10}B_0$ (a), $C_{10}B_{15}$ (b), $C_{10}B_{30}$ (c) and $C_{10}B_{45}$ (d) applicators. The clinical and geometrical axes are shown in red and black, respectively. The range of the electrons is decreased but isodoses remain almost parallel to the water surface.

3.1.1. Energy spectra at different depths

Table 3 shows differences in mean energy at the same depth for flat and 45° applicators. The deviations observed across different applicator diameters and energies are approximately 10%.

To illustrate this effect, a graphical representation of the normalized spectra of a flat and a 45° applicator compared to the initial discrete spectrum is shown in Fig. 8. The energy spectra drift towards low energies as the beveled

Table 3: The mean energy (E_z) at z_{max} is compared between different applicator/nominal energy combinations with a 45-degree bevel and the same depth in flat applicators. Here, $z_{0,45}$ represents the depth at which the average energy matches that of the inclined applicator at its z_{max}, when using the flat applicator. The final column presents correction factors for stopping-power ratios derived from Equation (9).

Applicator diameter d (cm)	Nominal energy (MeV)	z_{max} of C_dB_{45} (cm)	E_z C_dB_0 (MeV)	E_z C_dB_{45} (MeV)	E_z (C_dB_{45}) / E_z (C_dB_0)	$z_{0,45}$ (cm)	$S_{w,air}$ $(z_{0,45})$ / $S_{w,air}$ $(z_{max}C_dB_{45})$
10	12	0.73	7.98	7.12	0.89	1.25	1.010
10	10	0.72	6.90	6.08	0.88	1.21	1.011
10	8	0.48	5.41	4.81	0.89	0.83	1.009
10	6	0.29	4.32	3.80	0.88	0.56	1.008
5	12	0.73	7.81	6.96	0.89	1.19	1.009
5	10	0.65	6.82	6.08	0.89	1.06	1.009
5	8	0.48	5.35	4.73	0.88	0.84	1.009
5	6	0.29	4.30	3.79	0.88	0.57	1.008
3	12	0.68	8.14	6.96	0.85	1.33	1.013
3	10	0.60	7.17	6.51	0.91	0.96	1.008
3	8	0.48	5.55	4.99	0.90	0.79	1.007
3	6	0.29	4.43	4.01	0.90	0.52	1.003

angle is increased. The aforementioned energy changes can have an impact on absorbed dose determination using ionization chambers. Existing codes of practice [1, 2] depend on precalculated stopping-power ratios obtained from conventional linear accelerators, which are tabulated based on beam quality and depth. However, it should not be assumed that the stopping-power ratios remain valid for inclined applicators, even if previous studies have investigated changes in IOERT energy spectra for flat applicators and found a minimal effect on absorbed dose [10].

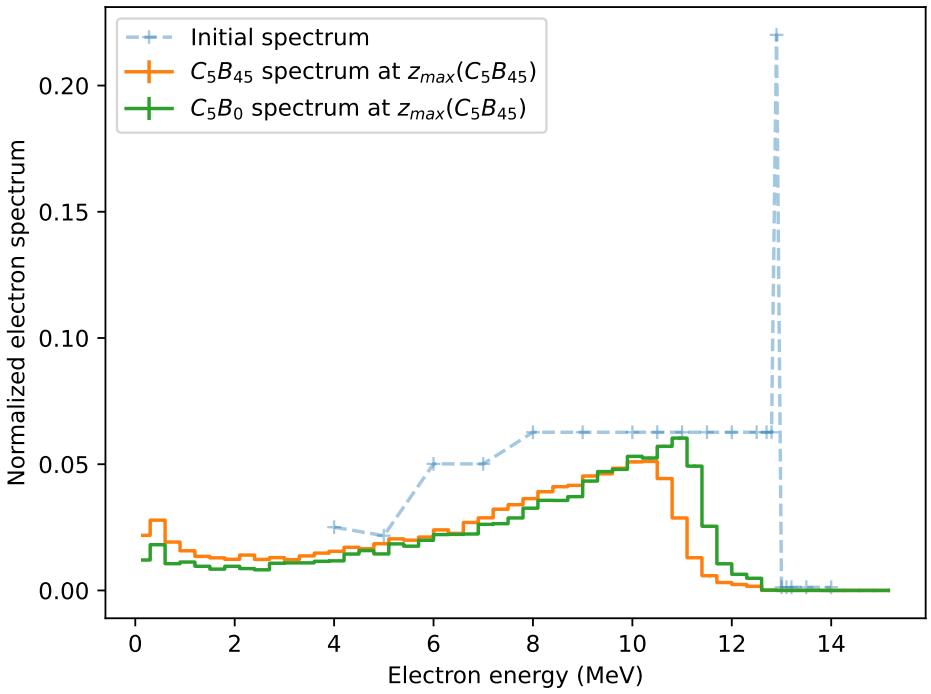

Fig. 8: Comparison of the initial spectrum (discrete) of a Monte Carlo simulated 12 MeV beam before hitting the scattering foil of the linac and the degraded spectra (electron only, binned) at z_{max} = 0.73 cm of the C_5B_{45} applicator and the same depth for the C_5B_0 applicator.

Fig. 9 depicts the variation of average electron energy with respect to depth, showcasing three different flat applicators and the four available beam energies.

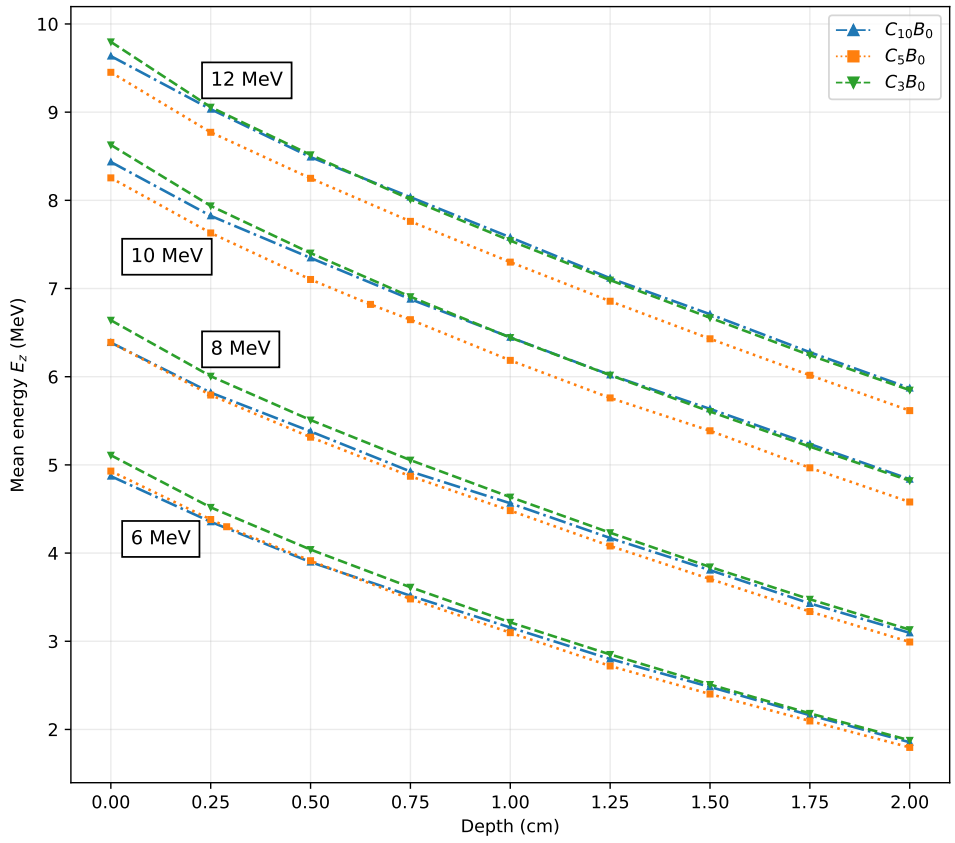

Fig. 9: Mean energy E_z as a function of depth along the clinical axis for $C_{10}B_0$, C_5B_0 and C_3B_0 applicators.

A comparison of the effect of the bevel angle on the mean energy of a 12 MeV beam with depth is depicted in Fig. 10. As the bevel angle increases,

the curves depicting mean energy versus depth begin to diverge. At z_{max} for the $C_{10}B_{45}$ applicator (z_{max}=0.73 cm), the differences in mean energy compared to the $C_{10}B_0$ applicator are approximately 10%. However, as the depth increases to 2 cm, the differences in mean energy exceed 20%. These results should be taken into account when considering the conversion from ionization to dose in PDD measurements with ionization chambers.

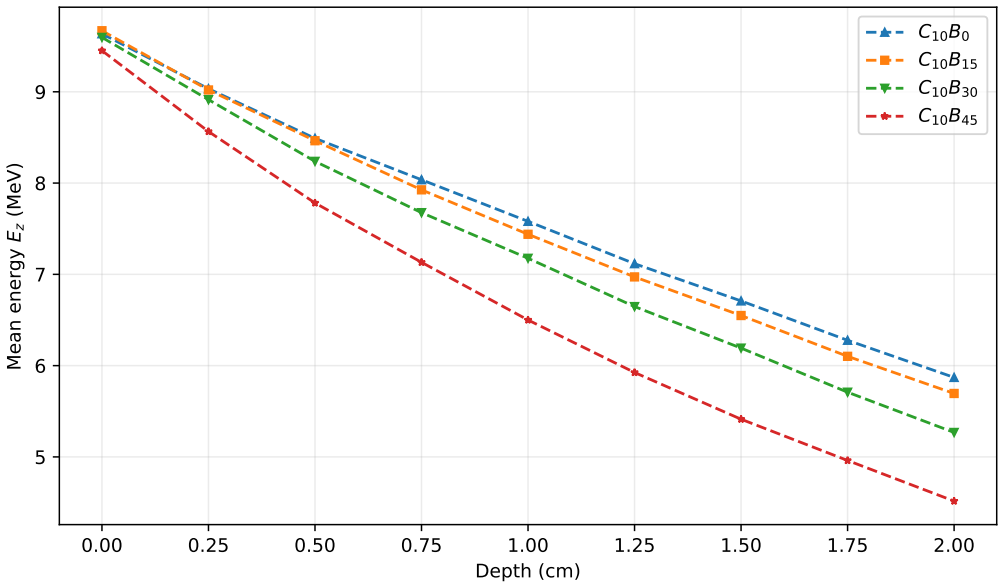

Fig. 10: Mean energy as a function of depth in the clinical axis for absorbed dose distributions in water with four different bevel angles using a 12 MeV beam and a 10 cm diameter applicator. The plot illustrates the accelerated decrease in mean energy with depth as the bevel angle is increased.

3.1.2. Correction factors for ionization chamber measurements

$z_{0,45}$ is calculated from mean energies of Table 3 for the 45° applicators and the variation of mean energy with depth in flat applicators from Fig. 9.

The proposed correction factors from Equation (9) for the 45° applicator are expressed in the last column of Table 3. It is worth noting that these correction factors can vary and, in some cases, reach as high as 1%.

3.2. Bevel factors

Fig. 11 presents comparisons of bevel factors calculated with penEasy with those determined with CC01 ionization chamber and microDiamond detector.

The uncertainty of bevel factors determined with microDiamond detector, employing Equation (4) was found to be 0.4% (k=1), corresponding to a ratio of measurements with an associated uncertainty of 0.3% (k=1) [1]. The uncertainty in the determination of output factors with the CC01 ionization chamber in IOERT with mobile linacs has been assessed to be 2% (k=1) by Iaccarino et al. [11], if the long term stability of the linac is not taken into account. Additionally, Monte Carlo dose calculations have an associated statistical uncertainty of 0.25% (k=1), as mentioned earlier in the manuscript. The total uncertainty of Monte Carlo calculated output factors, according to Equation (2), was found to be 0.35% (k=1).

The data obtained from microDiamond (without correction), and Monte Carlo demonstrate a satisfactory level of agreement (<1%). The CC01 measurements fall within a 2% range. However, applying the proposed correction factors for stopping-power ratios to CC01 measurements improves the overall agreement. Conversely, it is evident that the correction factors provided in Mastella et al. [20] fail to yield a satisfactory level of agreement.

To provide a comprehensive explanation for the significant variations observed in the corrected microDiamond bevel factors, it is beneficial to visually examine the absorbed dose distribution generated by an inclined applicator

and compare it to the scenario where the beam impinges on a water sphere at different angles (Fig. 12).

It is evident from Fig. 12 that when the beam impinges obliquely on the detector in a spherical medium, it generates a dose distribution with a steep gradient within the sensitive volume of the detector. In contrast, as previously discussed in this paper, the isodoses remain parallel to the water surface when utilizing oblique applicators.

Such situations are not directly comparable, resulting in distinctly different behaviors of the detector.

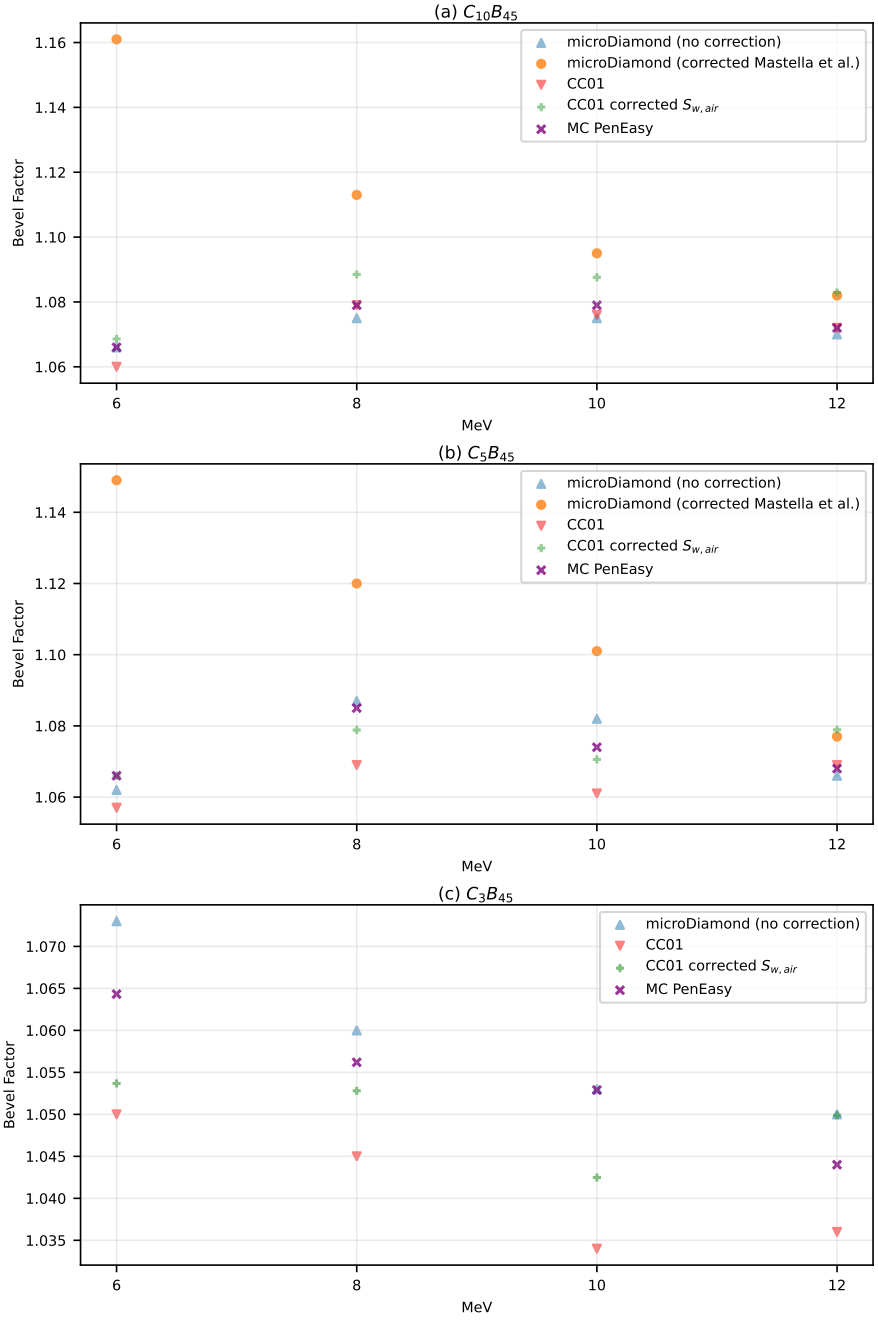

Fig. 11: Comparison of bevel factors for the $C_{10}B_{45}$ (a), C_5B_{45} (b) and C_3B_{45} applicators with different detectors and correction factors at the four nominal energies. The microDiamond corrected measurements exhibit a divergent behavior at lower energies. No corrections have been proposed for the C_3B_{45} applicator.

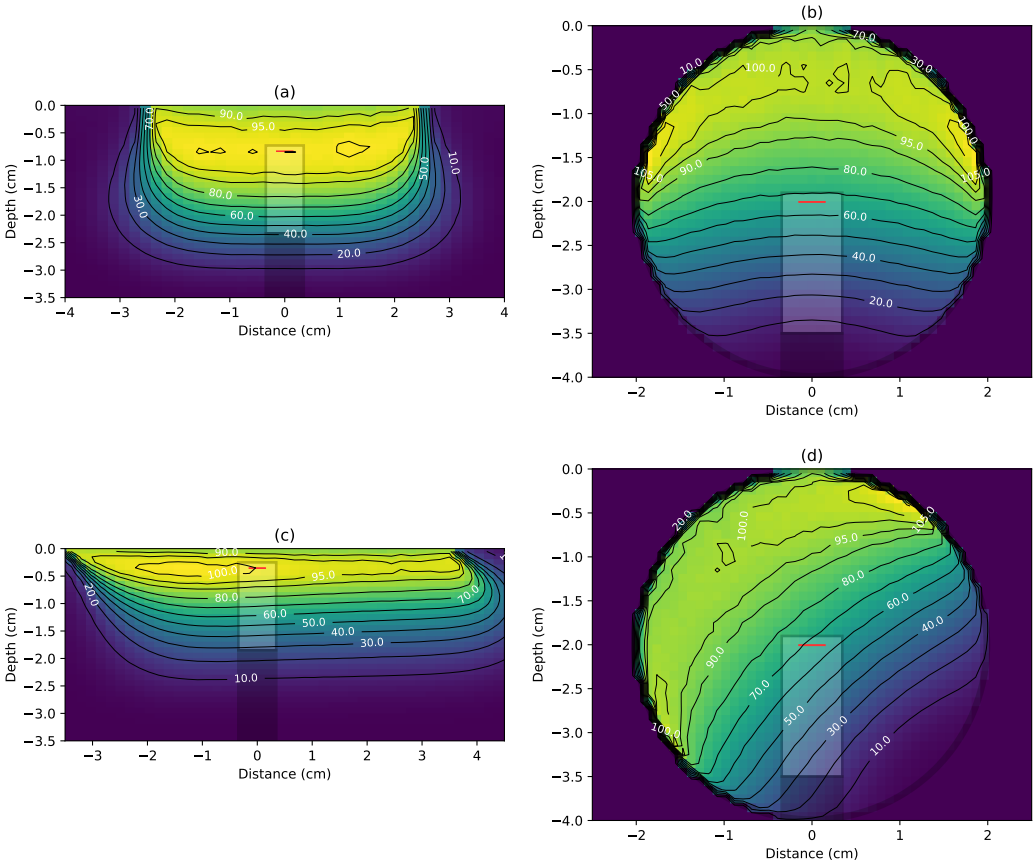

Fig. 12: Monte Carlo simulated isodose levels of a 6 MeV beam with C_5B_0 (a) and C_5B_{45} (c) applicators entering a flat water surface, compared to C_5B_0 impinging at 0° (b) and 45° (d) in a 4 cm diameter water sphere. A microDiamond schematic is superimposed on the dose distributions, with its sensitive volume shown in red (the thickness has been changed to 0.1 mm instead of 1 μm for better visibility).

4. Discussion

This study investigated bevel factors in IOERT using PTW microDiamond and IBA CC01 ionization chamber measurements, and compared them with penEasy simulations. The key findings of this research shed light on the correction factors required for accurate measurements with the microDiamond detector and the impact of changes in energy at z_{max} of beveled applicators on correction factors for ionization chamber measurements.

Firstly, our findings indicate that not applying angular response correction factors to microDiamond measurements significantly improves agreement with Monte Carlo simulations for all energies. Therefore, our study suggests that even if angular correction factors are deemed necessary, they should be minimal and inconsequential for achieving the accepted level of accuracy in clinical practice. Assuming that the electron fluence perturbation factor does not change between the field of interest and the reference field, the total uncertainty of bevel factor determination with the microDiamond detector was found to be 0.4% (k=1).

Secondly, the study found that variations in mean energy at z_{max} for beveled applicators significantly affect ionization chamber measurements. By applying correction factors to these measurements, we can mitigate a systematic discrepancy observed when comparing output factors determined with the microDiamond detector and Monte Carlo simulations. However, it has been shown that this issue also becomes relevant for all beveled applicators at greater depths and can potentially affect the shape of percentage depth dose curves.

Moreover, correction factors are energy-dependent, meaning that different types of mobile linacs will have different electron energy spectra and consequently different correction factors. Until these results are validated in

other IOERT accelerators, the use of the correction factors calculated in this study should be conditional upon the use of the same type of linac.

It is important to keep in mind that there is already a substantial challenge in accurately determining the k_{sat} values for cylindrical chambers in high dose per pulse beams, adding to the above-mentioned complications associated with ionization chamber measurements. Iaccarino et al. [11] reported an uncertainty of 2% (k=1) in the determination of output factors with cylindrical chambers, not taking into account the long term stability of the machine. Although that may be the case for flat applicators, we have found that an additional 1% (k=1) could be introduced if the change in mean energy for beveled applicators is not accounted for, resulting in a total uncertainty of 2.3% (k=1).

Given the above considerations, we recommend avoiding ionization chamber for determining output factors with inclined applicators. Instead, we propose the utilization of energy-independent detectors, such as the microDiamond, which has been validated in this study.

5. Conclusions

In conclusion, our work has led us to suggest that the use of microDiamond detectors for output factor measurements with inclined applicators in IOERT may not necessitate the application of angular response correction factors. This observation streamlines the dosimetry process, enhancing efficiency and accuracy during commissioning.

On the other hand, the study found that variations in electron mean energy at the depth of z_{max} of beveled applicators significantly affect ionization chamber measurements.

Based on these findings, we recommend the use of microDiamond detectors over ionization chambers for the determination of bevel factors in

IOERT mobile linacs. These results have significant implications for the clinical implementation of IOERT, and aim to contribute to the refinement of dosimetry protocols.

6. Declaration of Generative AI and AI-assisted technologies in the writing process

During the preparation of this work the authors used ChatGPT and Deepl Write in order to improve the readability of the text. After using this tools, the authors reviewed and edited the content as needed and take full responsibility for the content of the publication.

References

[1] INTERNATIONAL ATOMIC ENERGY AGENCY, Absorbed Dose Determination in External Beam Radiotherapy, rev. 1 Edition, Technical Reports Series, INTERNATIONAL ATOMIC ENERGY AGENCY, 2024. doi:10.61092/iaea.ve7q-y94k.
URL https://www.iaea.org/publications/15048

[2] P. R. Almond, P. J. Biggs, B. M. Coursey, W. F. Hanson, M. S. Huq, R. Nath, D. W. O. Rogers, AAPM's TG-51 protocol for clinical reference dosimetry of high-energy photon and electron beams, Medical Physics 26 (9) (1999) 1847–1870. doi:10.1118/1.598691.
URL http://doi.wiley.com/10.1118/1.598691

[3] R. F. Laitano, A. S. Guerra, M. Pimpinella, C. Caporali, A. Petrucci, Charge collection efficiency in ionization chambers exposed to electron beams with high dose per pulse, Physics in Medicine and Biology 51 (24) (2006) 6419–6436. doi:10.1088/0031-9155/51/24/009.
URL http://stacks.iop.org/0031-9155/51/i=24/a=009?key=crossref.f01d50c2f2f7196fd8947fe5dd5c3eaf

[4] F. Di Martino, M. Giannelli, A. C. Traino, M. Lazzeri, Ion recombination correction for very high dose-per-pulse high-energy electron beams: ksat

evaluation for very high dose-per-pulse electron-beams, Medical Physics 32 (7Part1) (2005) 2204–2210. doi:10.1118/1.1940167.
URL http://doi.wiley.com/10.1118/1.1940167

[5] A. Piermattei, S. D. Canne, L. Azario, A. Russo, A. Fidanzio, R. Miceli, A. Soriani, A. Orvieto, M. Fantini, The saturation loss for plane parallel ionization chambers at high dose per pulse values, Physics in Medicine and Biology 45 (7) (2000) 1869–1883. doi:10.1088/0031-9155/45/7/312.
URL https://iopscience.iop.org/article/10.1088/0031-9155/45/7/312

[6] E. Karaj, S. Righi, F. Di Martino, Absolute dose measurements by means of a small cylindrical ionization chamber for very high dose per pulse high energy electron beams: Small cylindrical chamber used in IORT dosimetry, Medical Physics 34 (3) (2007) 952–958. doi:10.1118/1.2436979.

[7] P. Björk, P. Nilsson, T. Knöös, Dosimetry characteristics of degraded electron beams investigated by Monte Carlo calculations in a setup for intraoperative radiation therapy, Physics in Medicine and Biology 47 (2) (2002) 239–256. doi:10.1088/0031-9155/47/2/305.

[8] P. Björk, T. Knöös, P. Nilsson, Measurements of output factors with different detector types and Monte Carlo calculations of stopping-power ratios for degraded electron beams, Physics in Medicine and Biology 49 (19) (2004) 4493–4506. doi:10.1088/0031-9155/49/19/004.
URL http://stacks.iop.org/0031-9155/49/i=19/a=004?key=crossref.611969377c674c2b9ca51dd968030983

[9] S. Righi, E. Karaj, G. Felici, F. Di Martino, Dosimetric characteristics of electron beams produced by two mobile accelerators, Novac7 and Liac, for intraoperative radiation therapy through Monte Carlo simulation, Journal of Applied Clinical Medical Physics 14 (1) (2013) 6–18. doi:10.1120/jacmp.v14i1.3678.

[10] M. Pimpinella, D. Mihailescu, A. S. Guerra, R. F. Laitano, Dosimetric characteristics of electron beams produced by a mobile accelerator for IORT, Physics in Medicine and Biology 52 (20) (2007) 6197–6214. doi:10.1088/0031-9155/52/20/008.

[11] G. Iaccarino, L. Strigari, M. D'Andrea, L. Bellesi, G. Felici, A. Ciccotelli, M. Benassi, A. Soriani, Monte Carlo simulation of electron beams generated by a 12 MeV dedicated mobile IORT accelerator, Physics in Medicine and Biology 56 (14) (2011) 4579–4596. doi:10.1088/0031-9155/56/14/022.

[12] G. X. Ding, D. W. O. Rogers, T. R. Mackie, Calculation of stopping-power ratios using realistic clinical electron beams, Medical Physics 22 (5) (1995) 489–501. doi:10.1118/1.597581.

[13] J. R. Palta, P. J. Biggs, J. D. Hazle, M. Huq, R. A. Dahl, T. G. Ochran, J. Soen, R. R. Dobelbower, E. C. McCullough, Intraoperative electron beam radiation therapy: Technique, dosimetry, and dose specification: Report of task force 48 of the radiation therapy committee, American Association of Physicists in Medicine, International Journal of Radiation Oncology*Biology*Physics 33 (3) (1995) 725–746. doi:10.1016/0360-3016(95)00280-C.
URL https://linkinghub.elsevier.com/retrieve/pii/036030169500280C

[14] A. S. Beddar, P. J. Biggs, S. Chang, G. A. Ezzell, B. A. Faddegon, F. W. Hensley, M. D. Mills, Intraoperative radiation therapy using mobile electron linear accelerators: Report of AAPM Radiation Therapy Committee Task Group No. 72: Task Group No. 72, Medical Physics 33 (5) (2006) 1476–1489. doi:10.1118/1.2194447.
URL http://doi.wiley.com/10.1118/1.2194447

[15] P. Björk, T. Knöös, P. Nilsson, Comparative dosimetry of diode and diamond detectors in electron beams for intraoperative radiation therapy, Medical Physics 27 (11) (2000) 2580–2588. doi:10.1118/1.1315317.
URL http://doi.wiley.com/10.1118/1.1315317

[16] M. Marinelli, G. Prestopino, C. Verona, G. Verona-Rinati, Experimental determination of the PTW 60019 microDiamond dosimeter active area and volume: PTW microDiamond active surface area and active volume, Medical Physics 43 (9) (2016) 5205–5212. doi:10.1118/1.4961402.
URL http://doi.wiley.com/10.1118/1.4961402

[17] C. Di Venanzio, M. Marinelli, A. Tonnetti, G. Verona-Rinati, M. Falco, M. Pimpinella, A. Ciccotelli, S. De Stefano, G. Felici, F. Marangoni, Characterization of a microDiamond detector in high-dose-per-pulse electron beams for intra operative radiation therapy, Physica Medica 31 (8) (2015) 897–902. doi:10.1016/j.ejmp.2015.06.008.
URL https://linkinghub.elsevier.com/retrieve/pii/S1120179715001489

[18] G. Güngör, G. Aydın, T. Z. Mustafayev, E. Özyar, Output factors of ionization chambers and solid state detectors for mobile intraoperative radiotherapy (IORT) accelerator electron beams, Journal of Applied Clin-

ical Medical Physics 20 (2) (2019) 13–23. doi:10.1002/acm2.12522.
URL http://doi.wiley.com/10.1002/acm2.12522

[19] O. J. Brace, S. F. Alhujaili, J. R. Paino, D. J. Butler, D. Wilkinson, B. M. Oborn, A. B. Rosenfeld, M. L. F. Lerch, M. Petasecca, J. A. Davis, Evaluation of the PTW microDiamond in edge-on orientation for dosimetry in small fields, Journal of Applied Clinical Medical Physics 21 (8) (2020) 278–288. doi:10.1002/acm2.12906.
URL https://onlinelibrary.wiley.com/doi/10.1002/acm2.12906

[20] E. Mastella, K. E. Szilagyi, E. De Guglielmo, S. Fabbri, F. Calderoni, A. Stefanelli, G. Di Domenico, A. Turra, Dosimetric characterization of a mobile accelerator dedicated for intraoperative radiation therapy: Monte Carlo simulations and experimental validation, Physica Medica 104 (2022) 167–173. doi:10.1016/j.ejmp.2022.11.006.

[21] E. Herranz, J. L. Herraiz, P. Ibáñez, M. Pérez-Liva, R. Puebla, J. Cal-González, P. Guerra, R. Rodríguez, C. Illana, J. M. Udías, Phase space determination from measured dose data for intraoperative electron radiation therapy, Physics in Medicine and Biology 60 (1) (2015) 375–401. doi:10.1088/0031-9155/60/1/375.
URL https://iopscience.iop.org/article/10.1088/0031-9155/60/1/375

[22] M. Marrale, A. Longo, G. Russo, C. Casarino, G. Candiano, S. Gallo, A. Carlino, M. Brai, Dosimetry for electron Intra-Operative Radio-Therapy: Comparison of output factors obtained through alanine/EPR pellets, ionization chamber and Monte Carlo-GEANT4 simulations for IORT mobile dedicate accelerator, Nuclear Instruments and Methods in Physics Research Section B: Beam Interactions with Materials and

Atoms 358 (2015) 52–58. doi:10.1016/j.nimb.2015.05.022.
URL https://linkinghub.elsevier.com/retrieve/pii/S0168583X15004930

[23] B. R. Muir, D. W. O. Rogers, Monte Carlo calculations of electron beam quality conversion factors for several ion chamber types: Electron beam k_Q factors, Medical Physics 41 (11) (2014) 111701. doi:10.1118/1.4893915.
URL http://doi.wiley.com/10.1118/1.4893915

[24] J. Sempau, P. Andreo, J. Aldana, J. Mazurier, F. Salvat, Electron beam quality correction factors for plane-parallel ionization chambers: Monte Carlo calculations using the PENELOPE system, Physics in Medicine and Biology 49 (18) (2004) 4427–4444. doi:10.1088/0031-9155/49/18/016.
URL http://stacks.iop.org/0031-9155/49/i=18/a=016?key=crossref.f55e54f6b583c39f201cad823316b34d

[25] J. W. Boag, E. Hochhäuser, O. A. Balk, The effect of free-electron collection on the recombination correction to ionization measurements of pulsed radiation, Physics in Medicine and Biology 41 (5) (1996) 885–897. doi:10.1088/0031-9155/41/5/005.
URL http://stacks.iop.org/0031-9155/41/i=5/a=005?key=crossref.7780bb090def6323ca63c38e01edc7a8

[26] B. R. Muir, D. W. O. Rogers, The central electrode correction factor for high-Z electrodes in small ionization chambers: Pcel calculated: High-Z, Medical Physics 38 (2) (2011) 1081–1088. doi:10.1118/1.3532818.

[27] I. Kawrakow, D. Rogers, E. Mainegra-Hing, F. Tessier, R. Townson,

B. Walters, EGSnrc toolkit for Monte Carlo simulation of ionizing radiation transport (2000).
URL https://doi.org/10.4224/40001303doi:10.4224/40001303[releasev2021]

[28] J. Sempau, A. Badal, L. Brualla, A PENELOPE-based system for the automated Monte Carlo simulation of clinacs and voxelized geometries–application to far-from-axis fields, Med. Phys. 38 (2011) 5887 – 5895. doi:10.1118/1.3643029.

[29] Nuclear Energy Agency, PENELOPE 2018: A Code System for Monte Carlo Simulation of Electron and Photon Transport: Workshop Proceedings, Barcelona, Spain, 28 January – 1 February 2019, PENELOPE: A Code System for Monte Carlo Simulation of Electron and Photon Transport, OECD, 2019. doi:10.1787/32da5043-en.

[30] J. Almansa, F. Salvat-Pujol, G. Díaz-Londoño, A. Carnicer, A. M. Lallena, F. Salvat, PENGEOM —A general-purpose geometry package for Monte Carlo simulation of radiation transport in material systems defined by quadric surfaces, Computer Physics Communications 199 (2016) 102–113. doi:10.1016/j.cpc.2015.09.019.
URL https://linkinghub.elsevier.com/retrieve/pii/S0010465515003707

[31] D. T. Burns, G. X. Ding, D. W. O. Rogers, R_{50} as a beam quality specifier for selecting stopping-power ratios and reference depths for electron dosimetry, Medical Physics 23 (3) (1996) 383–388. doi:10.1118/1.597893.